

Leveraging Real Fluid Effects as a Tool for Power Flow Measurements in 4 K Cryocooler Regenerators

R. Snodgrass¹, V. Kotsubo², J. Ullom^{1,2}, and S. Backhaus^{1,2}

¹National Institute of Standards and Technology, Boulder, CO 80305

²Department of Physics, University of Colorado Boulder, Boulder, CO 80309

ABSTRACT

The real fluid properties of helium have a major impact on the thermodynamics of pulse tube and Gifford-McMahon cryocoolers operating below about 30 K. For example, real fluid properties cause the temperature profile in a low-temperature regenerator to be nearly constant at the cold end and allow heat to be applied at warmer, intermediate points along the regenerator axis without affecting cooling power at the cold heat exchanger. We leverage these unique properties and the injection of intermediate heat as a tool for probing and validating the total power equation. As an initial demonstration of this technique, we show how it can be used to measure steady mass flow through the regenerator. We also discuss and demonstrate more advanced measurement protocols that may be used to isolate other terms responsible for power flow in low-temperature regenerators.

INTRODUCTION

The second-stage regenerators of low-frequency pulse tube or Gifford McMahon refrigerators commonly span temperatures between about 50 K and 4 K where thermophysical properties of helium vary dramatically. At these temperatures and at pressures near 1 MPa, helium no longer behaves as an ideal gas but rather as a real fluid. In a real fluid, enthalpy change dh depends upon both temperature and pressure changes:

$$dh = c_p dT + \frac{(1 - T\beta)}{\rho} dp, \quad (1)$$

where T is temperature, c_p is the isobaric specific heat, ρ is density, p is pressure, and β is the thermal expansion coefficient. Mean temperature T_m multiplied by β is highly temperature dependent (Fig. 1). For an ideal gas, $1 - T_m\beta = 0$, but for real fluids $1 - T_m\beta$ can be greater than zero ($T_m < 6.8$ K at mean pressure $p_m = 1.05$ MPa) or less than zero ($T_m > 6.8$ K). Depending on T_m , a pressure change creates a positive or negative change in enthalpy. The variety and unique shape of temperature profiles in low-temperature regenerators¹⁻³ can be understood by considering $T_m\beta$ and its influence on power flow.

To analyze the power flow we turn to the thermoacoustic framework pioneered by Rott⁴ and further developed by Swift.⁵ For a real fluid in a regenerator with finite solid heat capacity, the total power equation may be written⁶

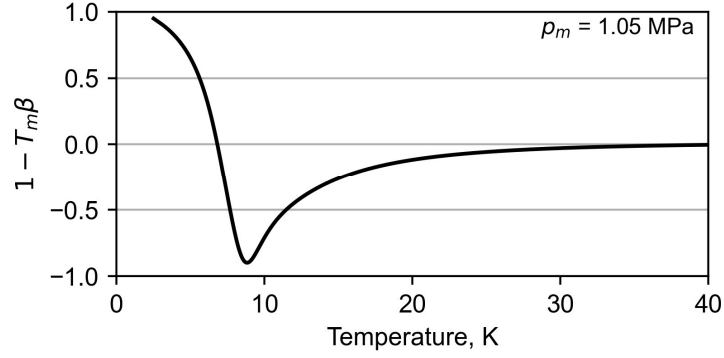


Figure 1. One minus temperature (T_m) multiplied by the thermal expansion coefficient (β) of helium-4 at a mean pressure 1.05 MPa.

$$\begin{aligned} \dot{H}_2(x) = \frac{1}{2} \text{Re} \left[p_1 \bar{U}_1 \left(1 - \frac{T_m \beta (f_\kappa - \tilde{f}_v)}{(1 + \epsilon_s)(1 + \sigma)(1 - \tilde{f}_v)} \right) \right] + F(x, T_m) |U_1|^2 \frac{dT_m}{dx} \\ - (A_g k + A_s k_s) \frac{dT_m}{dx} + \dot{N} h_{mol}. \end{aligned} \quad (2)$$

Here, p_1 and U_1 are complex amplitudes of the oscillating pressure and volumetric flowrate, σ is the Prandtl number, and $\epsilon_s = \phi \rho c_p / (1 - \phi) \rho_s c_s$ is the ratio of the fluid to solid volumetric heat capacities in the regenerator (ϕ, ρ_s, c_s are porosity, solid density, and solid specific heat, respectively). A tilde over a parameter signifies the complex conjugate. For brevity in Eq. 2 we have collected parameters that depend on material, geometry, and temperature in the $|U_1|^2 dT_m/dx$ term into $F(x, T_m)$:

$$F(x, T_m) = \frac{\rho c_p}{2A_g \omega (1 - \sigma) |1 - f_v|^2} \text{Im} \left[\tilde{f}_v + \frac{(f_\kappa - \tilde{f}_v)(1 + \epsilon_s f_v / f_\kappa)}{(1 + \epsilon_s)(1 + \sigma)} \right], \quad (3)$$

where f_κ and f_v are thermoacoustic functions that are known⁵ for a variety of regenerator geometries and ω is the angular frequency of the oscillating terms.

In Eq. 2, the first term is connected to the flow of acoustic power $\dot{E}_2 = \text{Re}[p_1 \bar{U}_1]/2$. The $|U_1|^2 dT_m/dx$ term carries power when there is an oscillating volume flow rate along a temperature gradient. The third term accounts for conduction, both through the gas (area A_g and thermal conductivity k) and through the regenerator solid (area A_s and thermal conductivity k_s). The final term is power carried by non-oscillating, steady mass flow (also called streaming) that may be present in geometries that allow it (e.g. a double-inlet pulse tube refrigerator). In this term, \dot{N} is steady molar flow and h_{mol} is the specific molar enthalpy.

To gain more intuition, the $p_1 \bar{U}_1$ term in Eq. 2 can be simplified by separating it into components that strongly depend only on real fluid effects (i.e. containing $T_m \beta$) and components that depend on finite heat capacity effects (i.e. containing ϵ_s). In realistic regenerators r_h/δ_κ is of order 0.1, and expansion of the thermoacoustic functions f_κ and f_v in a parallel plate geometry (as an approximation to porous media regenerators), yields

$$\begin{aligned} \dot{H}_2(x) \approx (1 - T_m \beta) \dot{E}_2 + \left(\frac{\epsilon_s}{1 + \epsilon_s} \right) T_m \beta \dot{E}_2 + F(x, T_m) |U_1|^2 \frac{dT_m}{dx} \\ - (A_g k + A_s k_s) \frac{dT_m}{dx} + \dot{N} h_{mol}. \end{aligned} \quad (4)$$

Some useful conclusions can already be drawn from Eq. 4. At and near the cold end of a low-temperature regenerator, dT_m/dx is approximately zero. This observation has been made (or predicted) by several other researchers¹⁻³ and is consistent with our high-resolution measurements reported here. Equation 4 shows that \dot{H}_2 at the cold end must be transported by some combination of the two \dot{E}_2 terms and by the streaming term. At the cold end of the regenerator, h_{mol} is small,

so the streaming term is generally negligible leaving only the \dot{E}_2 terms. In a well-insulated regenerator, the power flow is constant along its axis ($d\dot{H}_2/dx = 0$), and the power flow at the warm end is the same as at the cold end. Near the warm end $(1 - T_m\beta)$ is nearly zero and the regenerator heat capacity is typically large ($\epsilon_s \sim 0$). These properties force most of the power flow to be carried by the other terms in Eq. 4, which results in significant temperature gradients near the warm end. Between the cold and warm ends the temperature profile must adjust to the changing thermophysical properties of the solid(s) and fluid to satisfy $\dot{H}_2(x) = \text{constant}$.

Deep understanding of regenerator performance requires deep understanding of the power equation. Although real fluid effects in these systems have been investigated previously,^{1,2} few of these studies have used the thermoacoustic approach, and they have not typically been supported with robust measurements. Our experimental setup – detailed in the next section – was motivated by the desire to validate the thermoacoustic total power equation in realistic low-temperature regenerators and to gain practical knowledge about cryocoolers. Leveraging the properties of real fluids in low-temperature regenerators, we demonstrate techniques to measure steady streaming flow. We also demonstrate more advanced techniques that isolate other power flow terms in Eq. 4.

EXPERIMENTAL METHODS

Our experiments are performed using a two-stage, commercial pulse tube refrigerator operating near 1.4 Hz. Along the second-stage regenerator we attached 20 pairs of copper clamps that serve as mounts for thermometry or as heat injection points (Fig. 2). The two halves of each clamp pair are drawn together with two UNC 4-40 stainless steel screws. The halves do not directly touch, so that they are thermally isolated from each other. The contact area between each clamp half and the regenerator shell is an azimuthal band only 1.27 mm thick and slightly less than 180 degrees around the circumference. This small thermal contact patch minimally effects the temperature profile along the regenerator axis.

Silicon diode thermometers are bolted to half of the clamps along one side of the regenerator providing a spatial resolution of about 1.5 cm (10 diodes total). Two additional diodes are bolted directly to the copper of the warm and cold heat exchangers. Using a single, manufacturer-calibrated diode thermometer, we calibrated all other diode thermometers to an accuracy of ± 25 mK at temperatures less than 25 K and to ± 75 mK for higher temperatures. Of the 20 clamp pairs, the remaining 10 may be used for heat injection. Into each of these clamp-halves we have machined a pocket and have epoxied a resistance heater into the pocket. Unless specified, heat is always applied evenly to both halves to avoid azimuthal variation. We have the capability to apply between 0 and 1.5 W (in 1 mW increments) of heat to each clamp pair. Each pair at different axial locations is independently controlled.

Copper clamps were also attached to the second-stage buffer tube. The clamps were of the same design as the regenerator clamps shown in Fig. 2, only scaled in size to match the buffer tube diameter. Eight silicon diodes measured the temperature of the buffer tube.

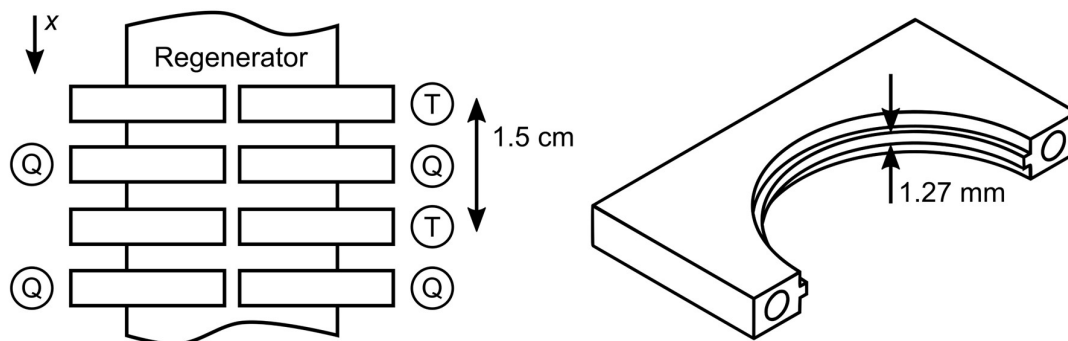


Figure 2. Experimental test setup. Two opposing pieces of copper clamp around the second-stage regenerator tube (side view, left, and isometric view of one piece, right). Half are used to measure temperature (T) and half are used to inject intermediate heat (Q). In most experiments presented here we only measure the temperature on one half of the regenerator.

In a typical experiment the cryocooler is cooled down and heaters and control loops on the warm and cold heat exchangers are used to reach desired warm end and cold end temperatures, T_w and T_c , which are maintained to the target temperatures ± 20 mK. Temperature profiles are recorded when the system reaches steady state. Then, heat is applied to one or more intermediate heat locations and the new temperature profile is recorded when the system reaches steady state again. Intermediate heat \dot{Q}_{int} is used as a tool to change the temperature profile and power flow in sections of the regenerator. Transient temperature data is also recorded for each thermometer at roughly 0.5 Hz. Oscillations in temperature at the frequency of the compressor are filtered by the temperature monitors to give the mean temperature T_m at each location.

RESULTS AND ANALYSIS

Key terms that determine the cooling power at the cold heat exchanger

Even in its simplified form in Eq. 4, the power flow equation is a complex combination of physical effects. We have performed a preliminary set of measurement showing that, under a restricted set of conditions that are often valid, the structure of the power flow equation at the cold heat exchanger is greatly simplified. Later in this paper, the conclusions that we can draw from this simplified form are used to create new techniques to directly probe the power in low-temperature regenerators.

Figures 3a and 3b show our measurements of the temperature profile of the regenerator and buffer tube, respectively, with no intermediate heat applied to the regenerator. With $T_c = 3$ K, the temperature profile is flat for almost half of the regenerator length and for about a third of the buffer tube length. The small temperature gradient at both ends of the cold heat exchanger makes the dT_m/dx power flow terms in Eq. 4 negligible at the cold end. On either side of the cold heat exchanger, we can simplify the total power flow in the regenerator $\dot{H}_{2,c}$ and in the buffer tube $\dot{H}_{2,bt}$ to

$$\dot{H}_{2,c} \approx (1 - T_c \beta_c) \dot{E}_{2,c} + \left(\frac{\epsilon_s}{1 + \epsilon_s} \right) T_c \beta_c \dot{E}_{2,c} + \dot{N} h_{mol,c}, \quad (5)$$

$$\dot{H}_{2,bt} \approx \dot{E}_{2,c} + \dot{N} h_{mol,c}. \quad (6)$$

Here, we simplified the power flow expression in the buffer tube by using the condition that the oscillations in the buffer tube are nearly adiabatic ($r_h \gg \delta_\kappa \sim \delta_\nu$). A First Law analysis at the cold heat exchanger (Fig. 4) shows that the cooling power \dot{Q}_c at that component is

$$\dot{Q}_c \approx \dot{E}_{2,c} T_c \beta_c \left(1 - \frac{\epsilon_s}{1 + \epsilon_s} \right). \quad (7)$$

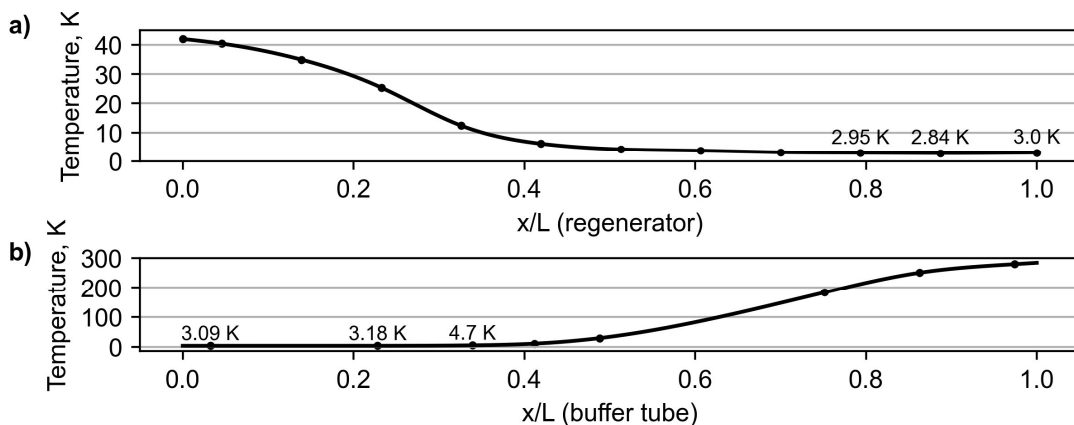


Figure 3. Temperature profile of the second-stage regenerator a) and buffer tube b) when the regenerator was regulated to 42 K at the warm end and 3 K at the cold end. Dots are thermometer measurements and lines are cubic spline fits to the measurements. No intermediate heat was applied.

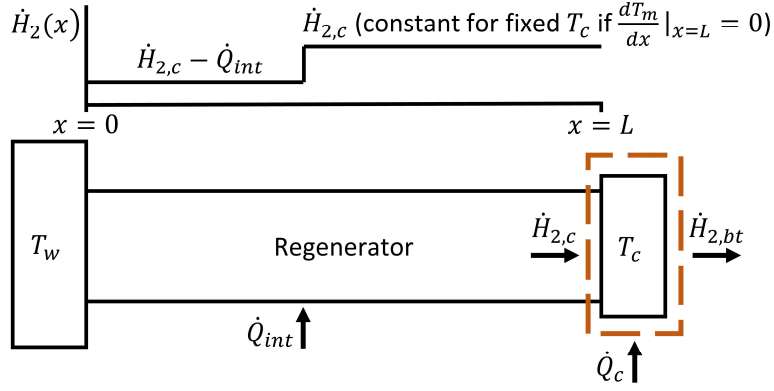


Figure 4. Schematic of the second-stage regenerator with intermediate heat applied. The top shows the idealized behavior of total power flow as a function of the distance x along the regenerator of length L . A control volume at the cold heat exchanger is used to determine that $\dot{H}_{2,c}$ is constant.

Before proceeding, we make a few additional comments on Eq. 7. As $T_c\beta_c$ approaches zero for $T_c < 7$ K, \dot{Q}_c drops rapidly. Finite regenerator solid heat capacity ($\epsilon_s \neq 0$) adversely affects cooling power, and very low solid heat capacity drives \dot{Q}_c to zero.

Changes in the cold and warm end power flows with intermediate heat

Previous work⁷⁻¹¹ shows that \dot{Q}_c is a constant even when substantial amounts of intermediate heat are applied to the regenerator. The inset in Fig. 5a shows our measurement of this behavior in our experimental system. With no intermediate heat applied to the regenerator, \dot{Q}_c of approximately 200 mW is required to reach $T_c = 3$ K. As the intermediate heat is swept from 0 W to 1.2 W, the \dot{Q}_c required to hold $T_c = 3$ K is nearly constant. This observation combined with Eq. 7 requires that $\dot{E}_{2,c}$ must be constant over this range of intermediate heat inputs ($T_c\beta_c$ and ϵ_s are fixed). Using this result in Eq. 5, we conclude that $\dot{H}_{2,c}$ is also constant over this range of intermediate heat applied to the regenerator.

We now analyze the power flows around a point of intermediate heat injection using a First Law control volume around this point. Since no heat injections occurs between this point and the cold heat exchanger, the power flow leaving the control volume to the right is $\dot{H}_{2,c}$. Therefore, \dot{H}_2 flowing into the control volume from the left is

$$\dot{H}_{2,w} = \dot{H}_{2,c} - \dot{Q}_{int}. \quad (8)$$

No heat is injected into the regenerator to the left of the control volume, and the power flow from the injection point to the warm heat exchanger is constant and equal to $\dot{H}_{2,w}$. If we hold T_c fixed and vary \dot{Q}_{int} , we are making known and controlled variations to the power flow to the left of the \dot{Q}_{int} injection point. \dot{Q}_{int} combined with our high-resolution temperature measurements becomes a tool to study and validate the power flow equation in Eq. 4.

Figures 5a and 5b show how this tool might be used and how the restrictions discussed above are met in practice. Fig. 5a shows the point of \dot{Q}_{int} injection at $x/L = 0.47$ (normalized distance along the regenerator axis) and measurements of the steady-state temperature profile for \dot{Q}_{int} up to 1.2 W. For these experiments, T_w was fixed at 42 K and T_c was regulated to 3 K. Over the entire range of \dot{Q}_{int} , the temperature gradient remains near zero at the cold end and $1 - T_c\beta_c$ remains of order 1, which show that our assumptions about the power flow in the regenerator near the cold heat exchanger are valid over this range. Measurement of the temperature profile in the buffer tube (not shown) did not show appreciable changes relative to Fig. 3b, demonstrating that our

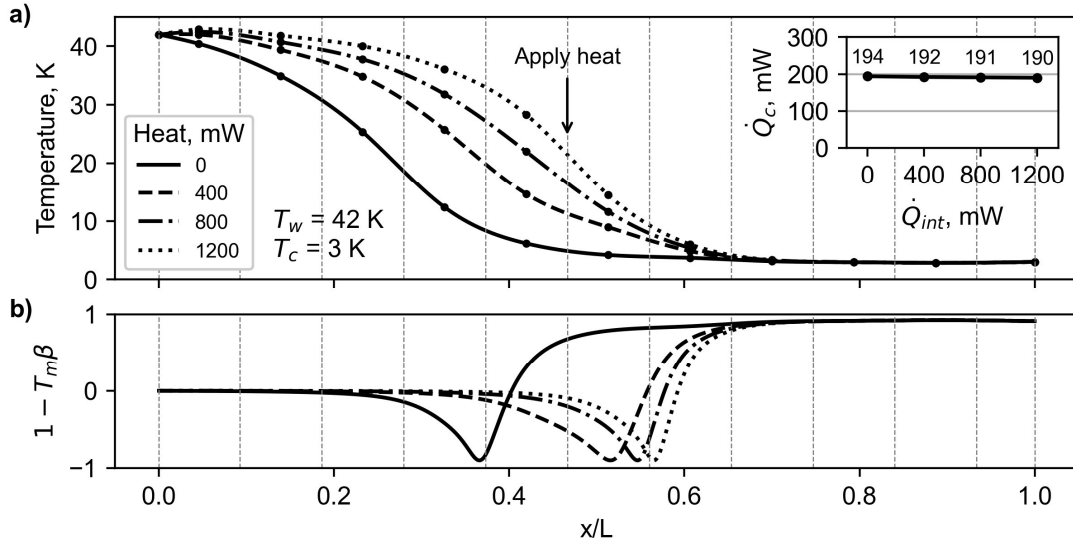


Figure 5. a) Steady state temperature profiles when different amounts of heat were applied at the location specified. Inset shows the cooling power at the cold end as a function of intermediate heat. Dotted vertical lines show all locations where heat could be applied given our system’s instrumentation. b) $1 - T_m \beta$ for the same temperature profiles shown in a). x/L is the normalized length along the regenerator.

assumptions regarding power flow in buffer tube are valid over this range. A critical observation from Fig. 5a is that as \dot{Q}_{int} is increased, $\dot{H}_{2,w}$ decreases (Eq. 8) and the temperature gradient at the warm end lessens so that the third and fourth terms in Eq. 4 carry less power.

A small complication at the point of intermediate heat injection

The schematic in Fig. 4 shows intermediate heat being applied to the regenerator in a step-like manner over zero distance. This is an idealization; in reality, heat must be conducted from the copper clamps to the stainless-steel regenerator tube, and then to the helium fluid and regenerator solid material. The finite heat transfer rate for all of these processes require some axial distance for \dot{Q}_{int} to migrate from the perimeter of the regenerator to its core so that the power flow becomes uniform across the cross section and can be modeled with the one-dimensional equations used throughout this paper.

To estimate the axial distance (“healing length”) for the power flow to become one dimensional, we applied a large amount of heat (1.5 W) at $x/L = 0.65$ to only one half of a copper clamp pair, leaving the other half unheated. We then recorded the temperatures of both halves of the regenerator at several upstream locations (closer to the warm heat exchanger), estimating that the power flow had returned to one dimensional once both halves were at the same temperature. In this test, the heat must migrate across an entire diameter of the regenerator. In all other experiments the heat only has to migrate from the perimeter to the center of the regenerator, so

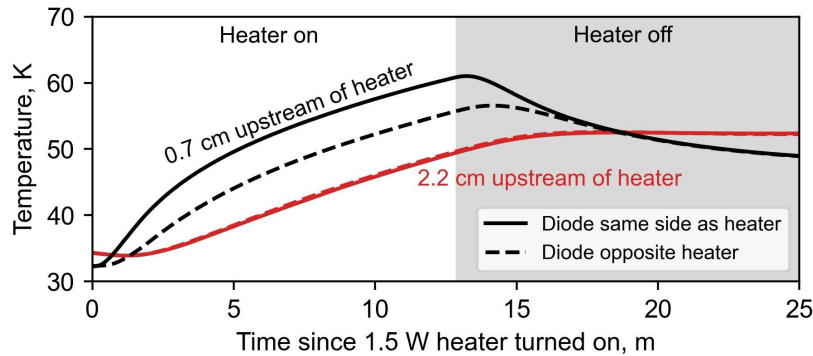


Figure 6. Evolution of temperature along the regenerator shortly after the helium compressor was turned off. At time = 0, an intermediate heat of 1.5 W was applied to one side of the regenerator to create an asymmetric heat input. Black and red lines are from diodes 0.7 cm and 2.2 cm upstream of the heater, respectively.

that this measurement results in an overestimate of the healing length. We also turned off the pressure and flow oscillations in the cryocooler, relying only on conduction and convection to transport heat across the regenerator diameter, leading to a further overestimate of the healing length.

The results are displayed in Fig. 6. At 0.7 cm upstream of the unbalanced heat injection, a significant temperature difference develops between the two regenerator halves. At 2.2 cm upstream, no temperature difference is observed. From the results of this test, it is likely acceptable to perform a one-dimensional analysis of $\dot{H}_2(x)$ at distances ≥ 2.2 cm upstream of the intermediate heat injection point.

Using real fluid effects to measure streaming through the regenerator

Returning to Eq. 4 and leveraging the analysis and preliminary tests described above, we describe a technique to measure the steady mass flow (streaming) through the regenerator. If sufficient \dot{Q}_{int} is injected, the temperature gradient at the warm end of the regenerator can be driven to zero while maintaining a cold end temperature gradient of zero. At the warm end, the helium is close to an ideal gas so that $1 - T_m\beta \sim 0$. The regenerator solid heat capacity is large compared to the helium so that ϵ_s is small at the warm end, but because \dot{E}_2 is large heat capacity effects should still be accounted for. Using these results and $dT_m/dx = 0$ at the warm and cold ends, Eq. 8 gives

$$\begin{aligned} & \left[\left(\frac{\epsilon_s}{1 + \epsilon_s} \right) T_m \beta \dot{E}_2 + \dot{N} h_{mol} \right]_{T_{flat}} + \dot{Q}_{int} \\ & \approx \left[(1 - T_m \beta) \dot{E}_2 + \left(\frac{\epsilon_s}{1 + \epsilon_s} \right) T_m \beta \dot{E}_2 + \dot{N} h_{mol} \right]_{T_c}, \end{aligned} \quad (9)$$

where T_{flat} is the temperature near T_w where the gradient is zero. Equation 9 can be rearranged into an expression for the molar steady flow

$$\dot{N} \approx \frac{\left[\left(1 - \frac{T_m \beta}{1 + \epsilon_s} \right) \dot{E}_2 \right]_{T_c} - \left[\left(\frac{\epsilon_s}{1 + \epsilon_s} \right) T_m \beta \dot{E}_2 \right]_{T_{flat}} - \dot{Q}_{int}}{h_{mol,flat} - h_{mol,c}}. \quad (10)$$

The measurements in Fig. 7 show that by injecting $\dot{Q}_{int} = 1.52$ W near the middle of the regenerator, we can force the temperature gradient at the warm end to zero. The acoustic power in Eq. 10 can be estimated using Eq. 7 and the measured \dot{Q}_c . The remaining variables can be computed from the known properties of helium and the regenerator solid. At present we do not know the regenerator solid materials used in this commercial cryocooler; however, if the material

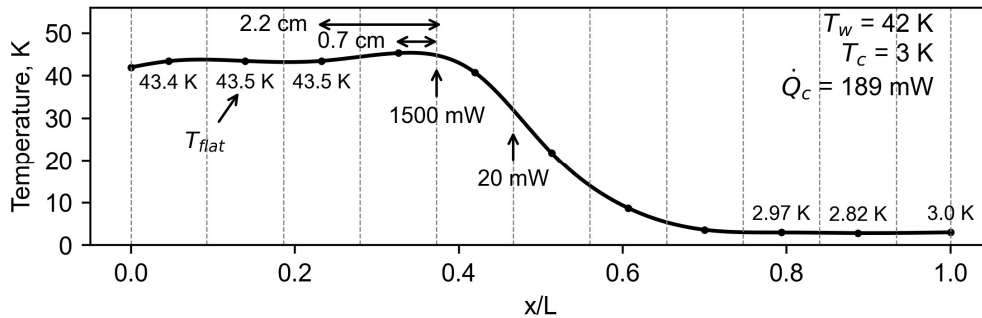


Figure 7. Regenerator temperature profile when 1.52 W of heat was applied to the locations shown by the arrows. Note that the temperature 0.7 cm upstream of \dot{Q}_{int} application is higher than the temperature 2.2 cm upstream. This is possibly an effect of underdeveloped \dot{H}_2 , as discussed in the previous section. T_{flat} is the temperature near the warm end where the gradient is zero.

at the cold end is HoCu_2 and the material at the warm end is Pb , then the streaming flow is 0.8 mmol/s .

Isolating temperature and temperature gradient terms of the total power equation

The experiments in Fig. 8 show how we can leverage and extend the results and techniques described above to examine individual terms in the total power equation. Here, we applied intermediate heat at two distinct locations labeled \dot{Q}_{sweep} and \dot{Q}_{control} . Extending the First Law analysis from Fig. 4 to this setting, \dot{Q}_{sweep} is used to vary the power flow by a known amount at the upstream location labeled “Measurement Plane”. Further upstream, \dot{Q}_{control} is used to adjust the temperature profile and fix either T_m or dT_m/dx at the Measurement Plane. The combination of these two intermediate heat injections gives the sensitivity of T_m or dT_m/dx to changes in power flow, which can be used to validate these terms in the power flow expression in Eq. 4.

In the specific experiment shown in Figs. 8a and 8b, the measurement plane is at $x/L \sim 0.6$, and we use \dot{Q}_{control} to fix T_m at 7.5 K . \dot{Q}_{sweep} is varied from 0 mW to 350 mW , and dT_m/dx is computed at the measurement plane using spline fits to the temperature measurements. The accuracy of the temperature control at the measurement plane is displayed in the Fig. 8a inset and in the middle plot in Fig. 8b. The measurements of \dot{Q}_c in bottom plot of Fig 8b and the temperature profiles near the cold end in Fig 8a show that this experiment stays within the range of validity discussed above, i.e. that $\dot{H}_{2,c}$ is constant.

The change in power flow at the measurement plane is the negative of the heat injection at the sweep injection point, i.e., $\Delta\dot{H}_2 = -\dot{Q}_{\text{sweep}}$. Since T_m is fixed at the measurement plane, the first two terms on the right hand side of Eq. 4 cannot adjust to generate $\Delta\dot{H}_2$: all of the variables in these terms are only a function of T_m , including \dot{E}_2 . The fifth term on the right hand side of Eq. 4 is the

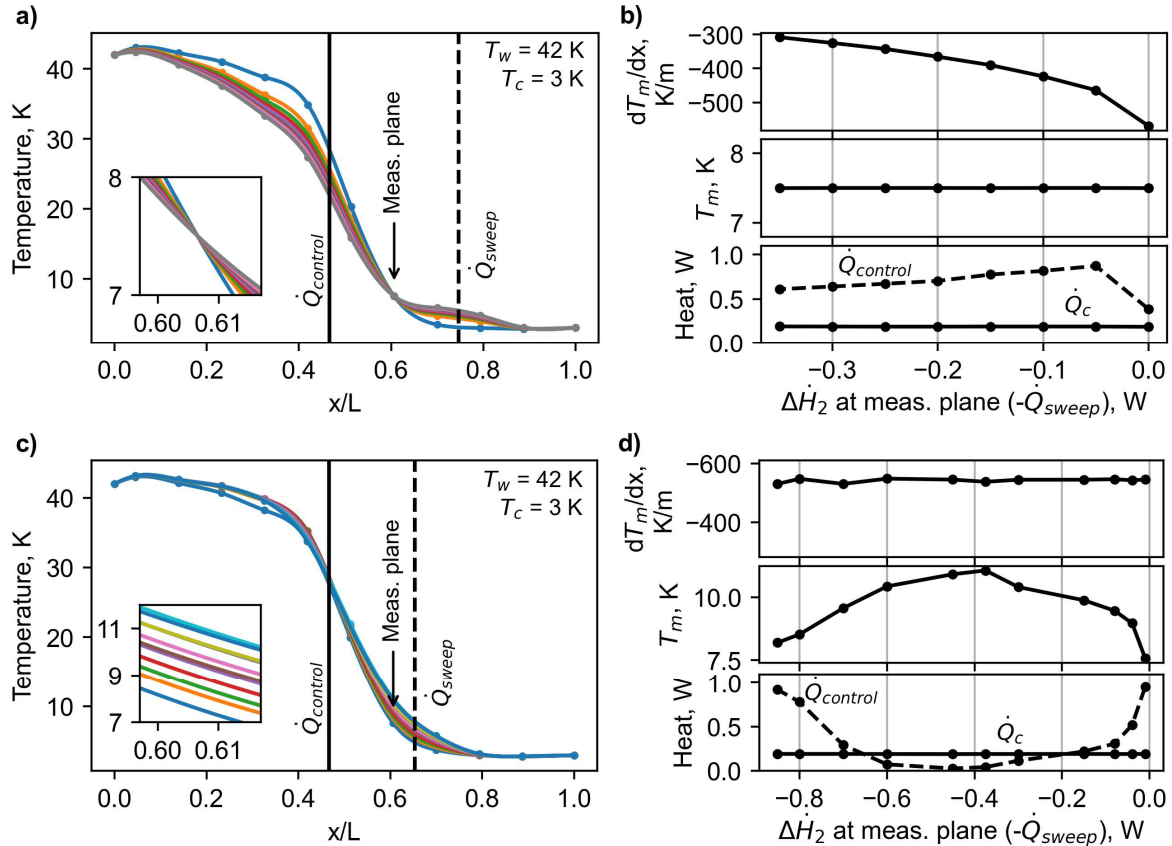


Figure 8. a) Temperature profiles of the regenerator when different amounts of sweeping heat were applied at the location of the vertical dashed line. Control heat was applied at the solid vertical line to keep the temperature at the measurement plane constant. Inset shows a zoom of the measurement plane. The temperature, temperature gradient, cooling power, and control heat for a) are shown as functions of the sweeping heat in b). c) and d) are similar except that temperature gradient was controlled.

power flow from steady streaming. This term does not adjust to generate $\Delta\dot{H}_2$ because the specific molar enthalpy is fixed by T_m and the streaming flow (N) is not significantly affected. The only remaining terms in Eq. 4 that can adjust are those proportional to dT_m/dx . Solid and fluid conduction in porous media regenerators are often negligible compared to the convection term in Eq. 4 (third term on the right hand side). Therefore, the power flow change at the measurement plane is approximately given by

$$-\dot{Q}_{sweep} = \Delta\dot{H}_2 \approx F(x, T_m) \Delta \left\{ |U_1|^2 \frac{dT_m}{dx} \right\}, \quad (11)$$

where $F(x, T_m)$ has been pulled outside of the $\Delta\{\dots\}$ because $F(x, T_m)$ should be constant for fixed T_m (see Eq. 3). We nominally expect \dot{Q}_{sweep} to be proportional to the change in dT_m/dx at the measurement plane. The top plot in Fig. 8b shows the trend for dT_m/dx versus $-\dot{Q}_{sweep}$. The general trend matches our expectation that reductions in \dot{H}_2 at the Measurement Plane results in a reduction in the magnitude of dT_m/dx . The relationship is relatively linear after the first reduction in total power, i.e. for $\Delta\dot{H}_2 < -0.05$ W.

We have considered two potential explanations for the nonlinear dependence between $\Delta\dot{H}_2$ and dT_m/dx . The first is related to the rapid changes in the compressibility of helium between 6 K and 8 K as it moves from liquid-like to ideal gas-like behavior. For the initial step in \dot{Q}_{sweep} , the helium between the measurement plane and the cold heat exchanger is in the liquid-like domain with very low compressibility, which leads to lower values of $|U_1|^2$ at the measurements plane and higher changes in dT_m/dx per $\Delta\dot{H}_2$. For the subsequent steps in \dot{Q}_{sweep} , the helium between the measurement plane and the cold heat exchanger is more toward the ideal gas compressibility, which leads to higher values of $|U_1|^2$ at the measurements plane and lower changes in dT_m/dx per $\Delta\dot{H}_2$. The second potential explanation of the nonlinear dependence between $\Delta\dot{H}_2$ and dT_m/dx is a transition to or from temperature asymmetry. As discussed in our group's companion paper at this conference,¹² large temperature asymmetries may exist between the two halves of the regenerator. In that case, it is not appropriate to assume $T_m(x)$ is azimuthally uniform, and the traditional thermoacoustic simplification of $\dot{H}_2(x)$ being one-dimensional no longer holds. In all future work we will attempt to restrict analyses like these to temperature profiles that we know are azimuthally symmetric, perhaps by influencing the profile with asymmetric intermediate heat.

Using the same methodology displayed in Figs. 8a and 8b, we have also controlled for constant dT_m/dx at the measurement plane while varying \dot{Q}_{sweep} . These experiments were performed before our improved understanding of the ‘‘healing length’’ requirement discussed above, and \dot{Q}_{sweep} was added just 0.7 cm from the measurement plane – too close to ensure the power flow is one dimensional. However, Figs. 8c and 8d demonstrate the feasibility of this technique and our ability to isolate the variation of T_m with $\Delta\dot{H}_2$ at the Measurement Plane.

CONCLUSION

Real fluid properties affect low-temperature cryocoolers in several important ways. As has been reported previously⁷⁻¹¹ and as we have found in our experiments, a sizable amount of intermediate heat can be applied to low-temperature regenerators without affecting cooling power at the cold heat exchanger (at least 1.52 W as shown by our study). The ability of the regenerator to absorb and transport this intermediate heat is derived from the flexibility in the temperature profile between the point of injection and the warm heat exchanger. Without intermediate heat applied, the temperature profile near the cold heat exchanger is flat and the temperature gradient is concentrated near the warm end. As intermediate heat is applied, the temperature gradient adjusts to changes in total power and, on average, becomes less steep.

Through analysis of the total power equation and measurements of the temperature profile, we showed that the power flow at the cold end is unaffected by injection of intermediate heat along the axis of the regenerator because the power flow into the cold heat exchanger is fixed by real fluid properties. The injected heat only modifies the power flow in the region between the injection point and the warm heat exchanger. This conclusion is dependent on the low-temperature

regenerator operating within a few bounds of validity: the cold end temperature stays fixed, the temperature gradient remains nearly zero on both the regenerator and buffer tube sides of the cold heat exchanger, and any steady streaming flow through the regenerator stays nearly constant. Our experiments demonstrate that these conditions are met for a wide range of intermediate heat injections.

Leveraging these observations, we developed several powerful techniques that use changes in intermediate heat input to isolate and measure individual terms in the power flow equation. Using a single intermediate heat injection, we forced the temperature gradient to zero at the warm heat exchanger and measured the power flow carried by steady streaming flow through the regenerator. Using two, spatially separated intermediate heat injections we demonstrated techniques to isolate and measure individual terms in the power flow equations, i.e., terms dependent on either dT_m/dx or T_m . In future work, we will improve the analysis and measurement presented here to validate the terms in the power equation – a particularly important goal, as cryocooler performance is inextricably tied to this equation.

ACKNOWLEDGMENTS

R. Snodgrass acknowledges support from a National Research Council Postdoctoral Fellowship. We also thank Greg Swift for stimulating discussion and leadership, and for assistance with the thermoacoustic software DeltaEC. We thank Ray Radebaugh for guidance during preliminary project planning, and Nathan Ortiz for experimental support.

Figures were generated using Matplotlib and material properties were gathered using CoolProp¹³, an open-source thermophysical library available as a Python wrapper.

Contribution of NIST, not subject to copyright.

REFERENCES

1. de Waele, A.T.A.M., Xu, M.Y., and Ju, Y.L., “Nonideal-gas effect in regenerators,” *Cryogenics*, vol. 39, no. 10, (1999), pp. 847–851.
2. Cao, Q., Qiu, L., and Gan, Z., “Real gas effects on the temperature profile of regenerators,” *Cryogenics*, vol. 61, (2014), pp. 31–37.
3. Lang, A., Häfner, H.-U., and Heiden, C., “Systematic Investigations of Regenerators for 4.2K-Refrigerators” in *Advances in Cryogenic Engineering*, Boston, MA: Springer US, pp. 1573–1580, (1998).
4. Rott, N., “Thermoacoustics” in *Advances in Applied Mechanics* vol. 20, Elsevier, pp. 135–175, (1980).
5. Swift, G.W., *Thermoacoustics: A Unifying Perspective for Some Engines and Refrigerators*, 2nd ed. Springer International Publishing, (2017).
6. Ward, B., Clark, J., and Swift, G., “Users Guide for DeltaEC: Design Environment for Low-amplitude Thermoacoustic Energy Conversion.” (2017), [Online]. Available: www.lanl.gov/thermoacoustics.
7. Ravex, A., Trolhier, T., Tanchon, J., and Prouvé, T., “Free Third-Stage Cooling for Two-Stage 4 K Pulse Tube Cryocooler,” in *Cryocoolers 14*, pp. 157–161, (2007).
8. Wang, C., “Extracting Cooling from the Pulse Tube and Regenerator in a 4 K Pulse Tube Cryocooler,” in *Cryocoolers 15*, pp. 177–184, (2009).
9. Prouvé, T., Godfrin, H., Gianèse, C., Triqueneaux, S., and Ravex, A., “Experimental results on the free cooling power available on 4K pulse tube coolers,” *J. Phys. Conf. Ser.*, vol. 150, no. 1, (2009), p. 012038.
10. Zhu, S., Ichikawa, M., Nogawa, M., and Inoue, T., “4 K pulse tube refrigerator and excess cooling power,” *AIP Conf. Proc.*, vol. 613, no. 1, (2002), pp. 633–640.
11. Uhlig, K., “³He/⁴He dilution refrigerator with high cooling capacity and direct pulse tube pre-cooling,” *Cryogenics*, vol. 48, no. 11, (2008), pp. 511–514.
12. Snodgrass, R., Kotsubo, V., Ullom, J., and Backhaus, S., “A Temperature Instability in 4 K Cryocooler Regenerators Caused by Real Fluid Properties,” *Cryocoolers 21*, (2021).
13. Bell, I.H., Wronski, J., Quoilin, S., and Lemort, V., “Pure and Pseudo-pure Fluid Thermophysical Property Evaluation and the Open-Source Thermophysical Property Library CoolProp,” *Ind. Eng. Chem. Res.*, vol. 53, no. 6, (2014), pp. 2498–2508.